



Research paper

Target Detection Using Multispectral Images, a Case Study: Wheat Detection in Chenaran County in Iran

*M. Imani**

Department of Telecommunication, Faculty of Electrical and Computer Engineering, Tarbiat Modares University, Tehran, Iran.

Article Info

Article History:

Received 25 May 2020
Reviewed 04 July 2020
Revised 30 September 2020
Accepted 03 November 2020

Keywords:

Target detection
Multispectral image
Wheat field
Attribute filter
Collaborative representation

*Corresponding Author's Email
Address:
maryam.imani@modares.ac.ir

Abstract

Background and Objectives: Target detection is one of the main applications of remote sensing. Multispectral (MS) images with higher spatial resolution than hyperspectral images are an important source for shape and geometric characterization, and so, MS target detection is interested.

Methods: A target detector appropriate for multispectral (MS) images is selected among hyperspectral target detectors and redefined in this paper. Many target detectors have been proposed for hyperspectral images in the remote sensing filed. Most of these detectors just use the spectral information. Since, the MS images have higher spatial resolution compared to hyperspectral ones, it is proposed that select a target detector that uses both of the spectral and spatial features. To this end, the attribute profile based collaborative representation (AP-CR) hyperspectral detector is chosen for MS images. Shape structures extracted by flexible attribute filters can significantly improve the MS target detection.

Results: As a case study, the wheat fields in Chenaran County in Iran are chosen as targets to be detected. The image acquired by Landsat 8 is used for doing experiment. The results show the superior performance of AP-CR with 96.09 % accuracy for wheat detection using MS image of Landsat 8.

Conclusion: The high performance of AP-CR is due to extraction of flexible attribute characteristics and the use of collaborative representation for approximation of each image pixel. Although the AP-CR method provides the highest accuracy, it needs a high running time compared to other detectors.

©2021 JECEI. All rights reserved.

Introduction

Identification and detection of target pixels such as man-made objects, special agriculture products and certain minerals is one of the main applications of remote sensing images. Target detection is interested among in various fields of agronomy, geology, mineralogy and so on [1], [2], [3] and [4]. Hyperspectral images by providing rich dimensionality for each pixel in the spectral domain allows for analyzing and discrimination of a variety of materials and land covers. A hyperspectral image is composed of hundreds images acquired in a wide range

of electromagnetic spectrum where a high spectral resolution about 10 nm can be provided. So, hyperspectral images with two spatial dimensions and a spectral dimension have a high capability in separation of targets from background. In addition to hyperspectral images, there are multispectral (MS) images that capture images from the ground in multiple (approximately about 10) spectral bands. Although MS images have lower spectral resolution compared to the hyperspectral images, but, they have higher spatial resolution that is important in characterization of shape, geometric and

spatial structures of objects of image [5], [6] and [7]. So far many target detectors have been introduced that most of them are applied for hyperspectral images. Table 1 provides a short review of them: Spectral matched filter (SMF) [8], Spectral angle mapper (SAM) [9], Matched subspace detector (MSD) [10], Orthogonal subspace projection (OSP) [11], Constrained energy minimization (CEM) [12], Adaptive subspace detector (ASD) [13], Sparsity based target detector (STD) [14], Kernel based SAM (KSAM) [15], Difference based target detection (DTD)-KSAM [16], Attribute profile based

collaborative representation (AP-CR) [17] and some other ones [18], [19], [20] and [21].

In this paper, we assess different hyperspectral target detectors to find which of them is appropriate for MS target detection. Since MS images have relatively high spatial resolution, AP-CR that utilizes the spatial information in addition to spectral one is selected for target detection.

AP-CR is a non-parametric approach with no need to estimate the data statistics.

Table 1: A short review of target detectors

Target detector	Year	Method
Spectral matched filter (SMF)	1992	A limiting case of generalized likelihood ratio test (GLRT) detector with simplified test statistic in the form of a normalized matched filter
Spectral angle mapper (SAM)	1993	It measures the spectral angle between the testing pixel and the spectral signature of target samples.
Matched subspace detector (MSD)	1994	An improved GLRT detector. Data is projected onto a low rank subspace to remove interference and remain signal. The image data projected onto the low rank subspace is matched to the image.
Orthogonal subspace projection (OSP)	1994	It projects the spectral vector of each pixel onto a subspace that is orthogonal to the undesired characteristics. It is an optimal process for interference suppression through the least squares approach.
Constrained energy minimization (CEM)	2000	It maximizes the response of the target signature while suppresses that of the undesired background.
Adaptive subspace detector (ASD)	2001	Based on theory of GLRT for adaption of MSD for unknown noise covariance matrices. It includes the adaptive cosine estimator (ACE) for situations that scaling of test samples may deviate from that of the training one.
Sparsity based target detector (STD)	2011	It sparsely approximate an image by a few target samples and also individually by using some background samples. Then reconstruction residuals are employed to obtain the output detection.
A supervised metric learning [18]	2014	A subpixel Target Detection for dealing with mixed signature of target spectrum and background pixels spectra through learning a distance metric.
A maximum margin metric learning [19]	2015	It transfers a hyperspectral target detection problem into a maximum margin problem.
Kernel based SAM (KSAM)	2016	The generalized version of SAM appropriate for nonlinear cases obtained by kernel function.
Median-mean line Reed-Xiaoli detector [20]	2017	An improved version of RX which utilizes the benefits of median-mean line metric.
Attribute profile based collaborative representation (AP-CR)	2018	It uses the attribute profiles for construction of target and background subspaces and then approximation of testing pixel based on target and background subspaces individually using collaborative representation. Then, reconstruction residuals are employed to obtain the output detection
Difference based target detection (DTD)-KSAM	2019	Output detection is result of difference between the distance of testing sample to the background signal and that to the target signal. KSAM is used as distance measurement.
A sparse and collaborative representation based detector [2]	2020	It utilizes the advantages of both sparse and collaborative representation for anomalous target detection.
Self-regularized weighted sparse model [21]	2021	An algorithm based on this hypothesis that data may come from multi-subspaces. It is proposed to detect infrared small targets in complex background.

It uses the benefits of attribute profile [22], [23] and collaborative representation (CR) [24], [25] to increase separation of targets from background using both of the spectral and spatial features. It redefined to use for MS images. One of the research domains in agriculture and geoscience field is detection of crop products such as wheat [26], [27] and [28]. Specially, in this paper, the AP-CR method is used for wheat detection using MS images acquired by Landsat 8 in Chenaran county fields in Iran.

Target Detector

Target detection algorithms have been often introduced for hyperspectral images. Hyperspectral images have a high spectral resolution that provide a worthwhile and useful source of spectral characteristics from background and targets. According to this reason, most of hyperspectral target detectors just use the spectral information while ignore the valuable spatial information. The spatial information can be very important for MS images that have lower spectral resolution and higher spatial resolution with respect to hyperspectral images. So, among different hyperspectral target detectors, the AP-CR method that uses the spatial information of images in addition to the spectral one is selected and redefined for MS target detection.

The geometrical structures and shape features have much perceptual significance that is useful for modelling of various objects and discrimination between different materials. Then, exploitation of these spatial features can be useful for different applications such as classification, object detection and target detection [29], [30]. Morphological operators, i.e., "opening" and "closing" filters by reconstruction extract spatial features such as shape characteristics and geometrical structures [31]. A structure element with a specific shape such as circle, rectangular and so on as a sliding window is considered in the morphological transformations. The extracted shapes and structures are substantially dependent on the shape of the considered structure element.

To extract structures with more generality that are not limited to some specific shapes, the attribute filters have been introduced. The attribute filters use one or several attributes instead of using a fixed structure element. Any attribute can be extracted from the image regions. The great flexibility in selection and defining the attributes allows a high capability for modelling of spatial information that are useful for discrimination of targets from background. The considered attributes can be textural such as standard deviation, entropy and range, geometric such as image moments, length of the perimeter, area, and shape factors, etc. Generally any measure computed from the image can be used as an attribute.

An Attribute profile (AP) is constituted through applying several attribute filters to a single band (gray level) image. The attribute filters merge connected components of the image at different levels. The filtering process is done as follows: a selected attribute denoted by a is calculated for each connected region R_i . The computed value indicated by $a(R_i)$ is then compared with a reference value λ . Two decision may be made [32]:

$a(R_i) \geq \lambda \rightarrow$ no change is applied to the connected region.

$a(R_i) < \lambda \rightarrow$ the grey level value of neighboring region with closer value is assigned to the connected region.

According to this approach, the neighboring connected components are merged. Merging with a neighboring region containing lower gray level is known as thinning and merging with the adjacent region of a higher gray level is called thickening. The attribute filters are applied to each band of MS individually and then, the filter outputs are stacked together to form the AP. Let consider m spectral bands for MS, s attributes and a sequence of thresholds $\{\lambda_1, \lambda_2, \dots, \lambda_n\}$. A thinning profile with attribute a_k is composed from applying a sequence of attribute thinning operators:

$$\begin{aligned} Thin_{a_k}(y_j) &= \{\gamma_n(y_j), \dots, \gamma_1(y_j)\}; \\ j &= 1, 2, \dots, m; k = 1, 2, \dots, s \end{aligned} \quad (1)$$

where γ_i indicates the thinning operator and y_j is the j th spectral band of MS image. Similarly, the thickening profile is generated by applying thickening operators:

$$\begin{aligned} Thick_{a_k}(y_j) &= \{\varphi_n(y_j), \dots, \varphi_1(y_j)\}; \\ j &= 1, 2, \dots, m; k = 1, 2, \dots, s \end{aligned} \quad (2)$$

where φ_i denotes the thickening operator. The extended thinning profile and the extended thickening profile of k th attribute are given, respectively by:

$$\begin{aligned} E_{Thin_{a_k}} &= \{Thin_{a_k}(y_1), Thin_{a_k}(y_2), \dots, Thin_{a_k}(y_m)\}; \\ k &= 1, 2, \dots, s \end{aligned} \quad (3)$$

$$\begin{aligned} E_{Thick_{a_k}} &= \{Thick_{a_k}(y_1), Thick_{a_k}(y_2), \dots, Thick_{a_k}(y_m)\}; \\ k &= 1, 2, \dots, s \end{aligned} \quad (4)$$

and finally the extended multi thinning profile and the extended multi thickening profile are provided as follows:

$$EM_Thin = \{E_Thin_{a_1}, E_Thin_{a_2}, \dots, E_Thin_{a_s}\} \quad (5)$$

$$EM_Thick = \{E_Thick_{a_1}, E_Thick_{a_2}, \dots, E_Thick_{a_s}\} \quad (6)$$

The extended multi thinning profile and the extended multi thickening profile are called for simplicity thinning profile and thickening profile, respectively. While the thinning profile contain the detail information of image, the thickening one has more homogeneous regions. From the other hand, thinning and thickening just contain the spatial features. To include the spectral features too, the MS bands are stacked to the thinning profile to compose the target subspace. Moreover, the spectral bands are stacked to the thickening profile to generate the background subspace. The obtained target and background subspaces are used for estimate of each testing pixel. An unknown pixel is approximated by each of target subspace and background subspace individually. The label of each subspace that can be better estimate the testing pixel is assigned to the testing pixel. So, a label of target or background is determined for each pixel of image. To approximate the pixel through a subspace, the collaborative representation (CR) method is used. According to this approach, each pixel can be approximated through a linear combination of samples of subspace where a distance weighted Tikhonov matrix is considered to adjust the contribution of each sample of the subspace. CR has two main advantages: 1- it is a nonparametric method for image modeling. In other words, it does not consider any assumption about statistical distribution of data, 2- due to using l_2 norm in the optimization problem, CR is simply implemented and achieves a closed form solution. By considering \mathbf{X}_b as the background subspace, estimate of the testing pixel denoted by \mathbf{y} is obtained by:

$$\hat{\mathbf{y}}_b = \mathbf{X}_b \hat{\mathbf{a}}_b \quad (7)$$

Similarly, by considering \mathbf{X}_t as the target subspace, the estimate of \mathbf{y} is given by:

$$\hat{\mathbf{y}}_t = \mathbf{X}_t \hat{\mathbf{a}}_t \quad (8)$$

where $\hat{\mathbf{a}}_b$ and $\hat{\mathbf{a}}_t$ are the weight vectors associated with the background and target subspaces, respectively. These weight vectors are computed through solving an optimization problem. For more explanations, the reader is referred to [17]. These vectors are obtained as follows:

$$\hat{\mathbf{a}}_b = (\mathbf{X}_b^T \mathbf{X}_b + \lambda_b \mathbf{\Gamma}_{y_b}^T \mathbf{\Gamma}_{y_b})^{-1} \mathbf{X}_b^T \mathbf{y} \quad (9)$$

$$\hat{\mathbf{a}}_t = (\mathbf{X}_t^T \mathbf{X}_t + \lambda_t \mathbf{\Gamma}_{y_t}^T \mathbf{\Gamma}_{y_t})^{-1} \mathbf{X}_t^T \mathbf{y} \quad (10)$$

where λ_b and λ_t are the regularization parameters and $\mathbf{\Gamma}_{y_b}$ and $\mathbf{\Gamma}_{y_t}$ are the Tikhonov matrices. These matrices are used to assign larger coefficients to more similar pixels to the testing pixel. In other words, they force that pixels of the subspace with more similarity to the testing pixel, have greater contribution in approximation of

testing pixel. The output of target detector is obtained by:

$$D(\mathbf{y}) = r_b(\mathbf{y}) - r_t(\mathbf{y}) \quad (11)$$

where $r_b(\mathbf{y})$ and $r_t(\mathbf{y})$ are the residual error of approximation computed in background and target subspaces, respectively:

$$r_b(\mathbf{y}) = \|\mathbf{y} - \hat{\mathbf{y}}_b\|_2 = \|\mathbf{y} - \mathbf{X}_b \hat{\mathbf{a}}_b\|_2 \quad (12)$$

$$r_t(\mathbf{y}) = \|\mathbf{y} - \hat{\mathbf{y}}_t\|_2 = \|\mathbf{y} - \mathbf{X}_t \hat{\mathbf{a}}_t\|_2 \quad (13)$$

Note that $D(\mathbf{y})$ is a scalar number assigned to each pixel \mathbf{y} . The values of $D(\mathbf{y})$ for all pixels of image is used to form a grey level image. A pseudo color image can be generated according to this grey level image where a larger value for a pixel indicates that the pixel belongs to the target class with a higher probability and a smaller value is corresponding to belonging to the background class. To generate a binary detection map, it is enough that consider a threshold value for target detection:

$$\text{if } D(\mathbf{y}) \geq \text{thr} \rightarrow \mathbf{y} \text{ is target}$$

$$\text{if } D(\mathbf{y}) < \text{thr} \rightarrow \mathbf{y} \text{ is background}$$

The block diagram of the proposed AP-CR method is shown in Fig.1.

Study area and Evaluation Measures

The study area is Chenaran County in Razavi Khorasan Province in Iran with the following geographic coordinates:

36° 34'45" N

59° 17'41" E

36° 47'27" N

58° 52'47" E

Chenaran is an agricultural city with many farms in the outskirts. The image is acquired by Landsat 8¹. An overview of the whole dataset is shown in Fig. 2. A part of this dataset, i.e., the region of Chenaran, is used for doing experiments in this work that the Google earth image of it is shown in Fig. 3. The grey level image of band 6 of Landsat 8 is also seen in Fig. 4. To assess the detection performance, the receiver operating characteristic (ROC) that plots a probability of detection P_d versus the false alarm rate R_f is used:

$$P_d = \frac{N_{cd}}{N_t} \quad (14)$$

and

$$R_f = \frac{N_{fd}}{N} \quad (15)$$

where N is the total number of image pixels and N_t is the total number of target pixels.

¹ <http://earthexplorer.usgs.gov>

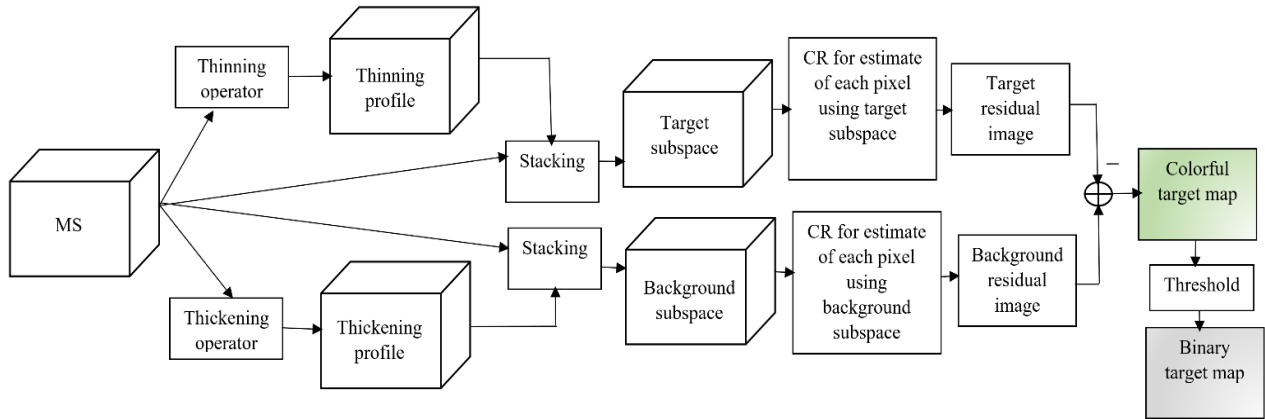


Fig. 1. Block diagram of the AP-CR method.

The number of pixels that are correctly detected is denoted by N_{cd} while the number of target pixels that are falsely detected is indicated by N_{fd} . Usually, in addition to plotting ROC, the area under curve (AUC) is computed. If a ROC curve be closer to the top left corner or its associated AUC has a higher value closer to 1, the detector has better performance. Some regions of wheat

fields are obtained through field operations as samples of the target class. The yellow regions shown in Fig. 5 are the wheat fields. The binary map of the target samples is also shown in Fig. 6. 10% of these regions are randomly selected and used as training samples. The chosen training samples are shown in Fig. 7. Similarly, 10% of background regions are used as background training samples.

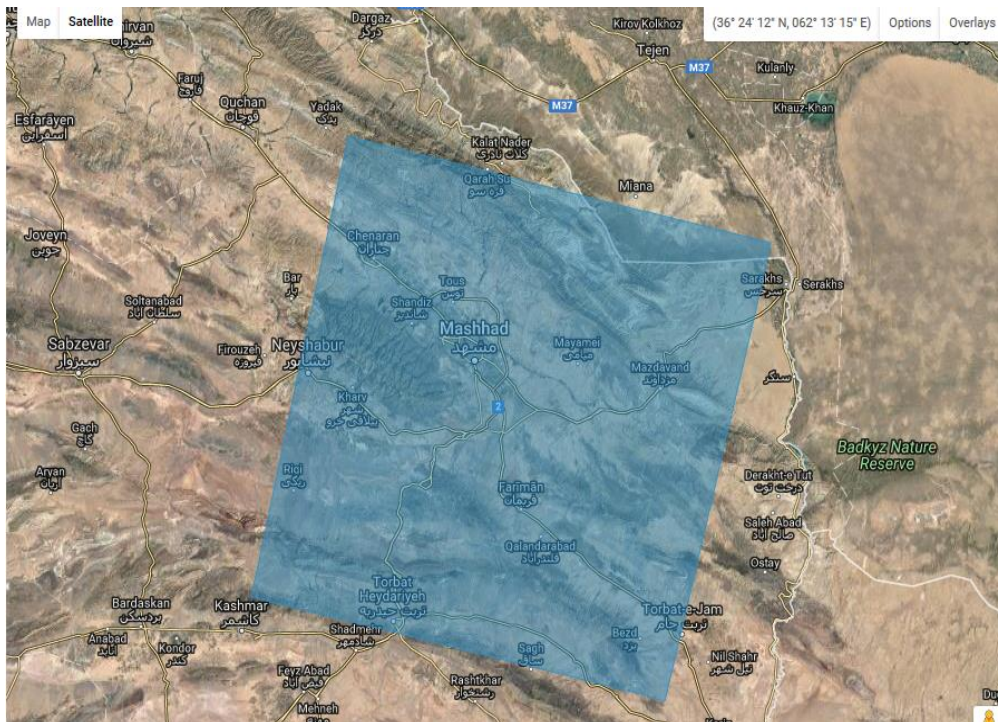


Fig. 2. An overview of Landsat 8 image outskirts of Chenaran County.



Fig. 3: Google earth image of the study area in Chenaran.



Fig. 4: Grey level image of band 6 of Landsat 8 of the study area in Chenaran.



Fig. 5: Some wheat fields as samples.



Fig. 6: Binary map of target regions.

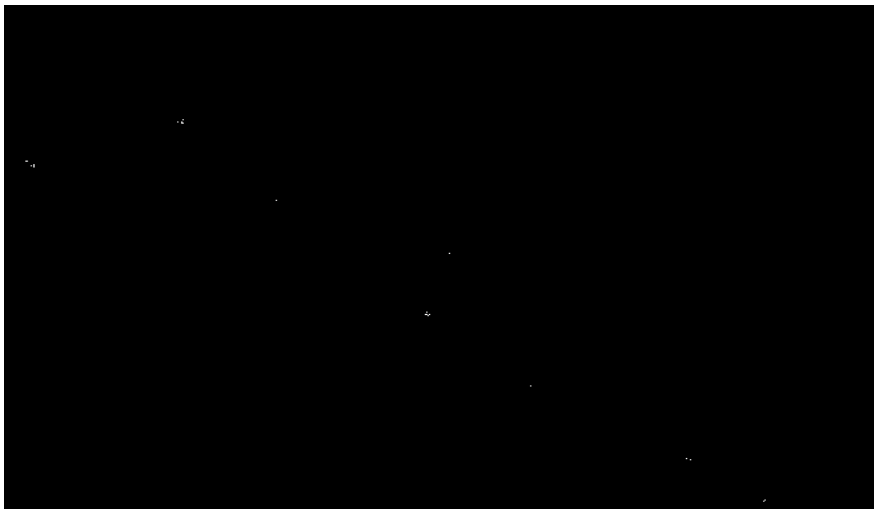


Fig. 7: Chosen training samples.

Results and Discussion

The detectors are firstly divided into two groups. The first group consists of the popular and widely used detectors (SMF, MSD, ASD, OSP, SAM, KSAM, CEM and STD).

The second group consists of two state-of-the-art recently detectors (DTD-KSAM and AP-CR). In the first experiment, the first group of detectors are applied to the MS image.

The AUC values in addition to the running time are reported in [Table 2](#). Among different methods of this group, CEM, SAM and KSAM provide the best results, respectively. STD despite spending the highest running time could not provide desired results. The ROC curves of different detectors of the first group are plotted in [Fig. 8](#). The detection map of the first rank methods are shown in [Fig. 9](#).

The map of wheat cover is obtained through Google earth monitoring.

Then, it is corrected according to field operations. The result map is shown in [Fig. 10](#) where wheat fields are illustrated with green color in the image. It can be used as a reference for comparison of the obtained target maps.

The different images obtained by applying thinning filters and thickening ones used in AP-CR method for composing the target and background subspaces are shown in [Fig. 11](#). In addition, the target residual image and the background residual image are shown in [Fig. 12](#). In the second experiment, the DTD-KSAM and AP-CR are assessed for wheat detection.

The comparison results (AUC and time) are reported in [Table 3](#). As seen, AP-CR significantly works better than DTD-KSAM for wheat detection using MS image of Landsat 8. To have a conclusion of the detection results, the AUC and running time of the best detectors of the first group are shown beside the DTD-KSAM and AP-CR detectors in [Table 4](#).

The results show that AP-CR is the best method although it needs the highest running time.

The high complexity of AP-CR is due to 1- applying the attribute filters and 2- solving the optimization problem in the collaborative representation for approximation of each image pixel.

As said before, the high ability of AP-CR is because of using valuable spatial features in addition to the spectral ones. Other competitor detectors, i.e., SAM, KSAM, CEM and DTD-KSAM just use the spectral information of the MS image. To assess the performance of these detectors in presence of spatial features, we do an experiment. In this experiment, a morphological profile containing 7 “opening” filters and 7 “closing” filters is constituted and then stacked on the original MS image to form a spectral-spatial cube.

Then, the obtained cube is fed to the SAM, KSAM, CEM, DTD-KSAM and AP-CR detectors as the input. The results are reported in [Table 5](#) and the ROC curves are shown in [Fig. 13](#).

The detection maps are also illustrated in [Fig. 14](#). By comparison between the results of [Table 4](#) (obtained by just the spectral features) and the results of [Table 5](#) (obtained by the spectral and spatial features), it can be concluded that the SAM, KSAM and CEM detectors can provide better results when both of the spectral and spatial features are used.

But, efficiency of DTD-KSAM and AP-CR without using morphological features is better than when they are used.

Note that, AP-CR has itself spatial features obtained by attribute filters and when this detector is applied to a cube of spectral and spatial features of morphological profile, a redundancy of spatial information is generated that degrades the performance of AP-CR.

However, by a comparison among all detectors of [Table 4](#) and [5](#), it is found that the AP-CR method by using the MS image containing spectral features is the best detector with the highest AUC value.

In the following, by selection of AP-CR as the appropriate target detector for MS images, the binary detection map is generated.

Table 2: AUC values and running time of different detectors in the first group

Method	SMF	MSD	ASD	OSP	SAM	KSAM	CEM	STD
AUC	55.85	49.98	49.23	19.50	70.54	69.21	82.51	50.00
Computation time (seconds)	11.24	17.16	20.43	6.43	8.41	40.92	52.19	30142.19

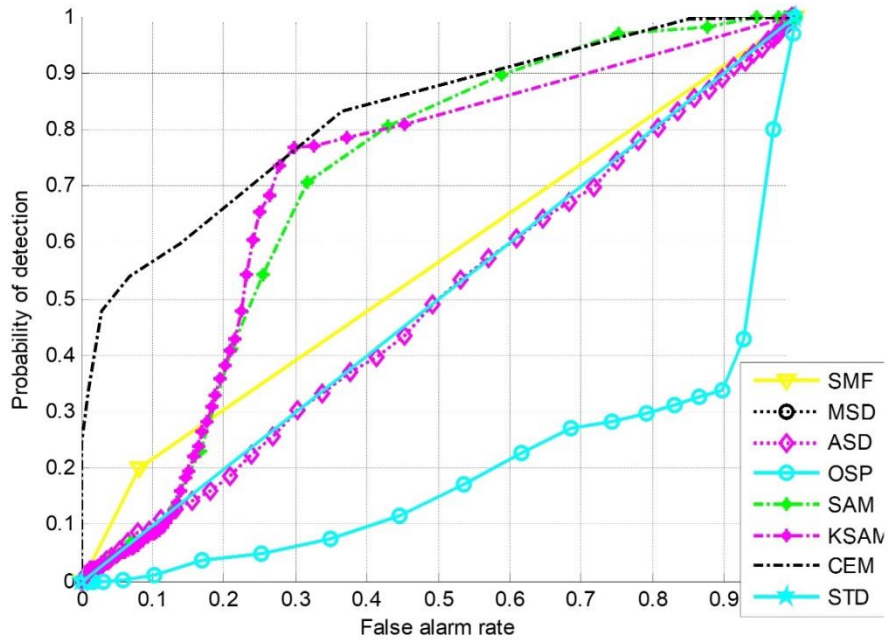


Fig. 8: ROC curves of different methods of the first group of detectors.

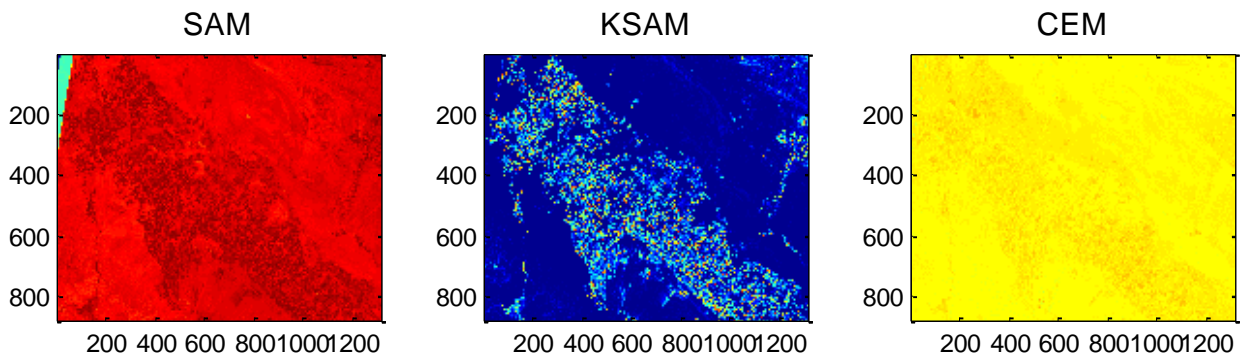


Fig. 9: Detection maps of SAM, KSAM and CEM detectors.

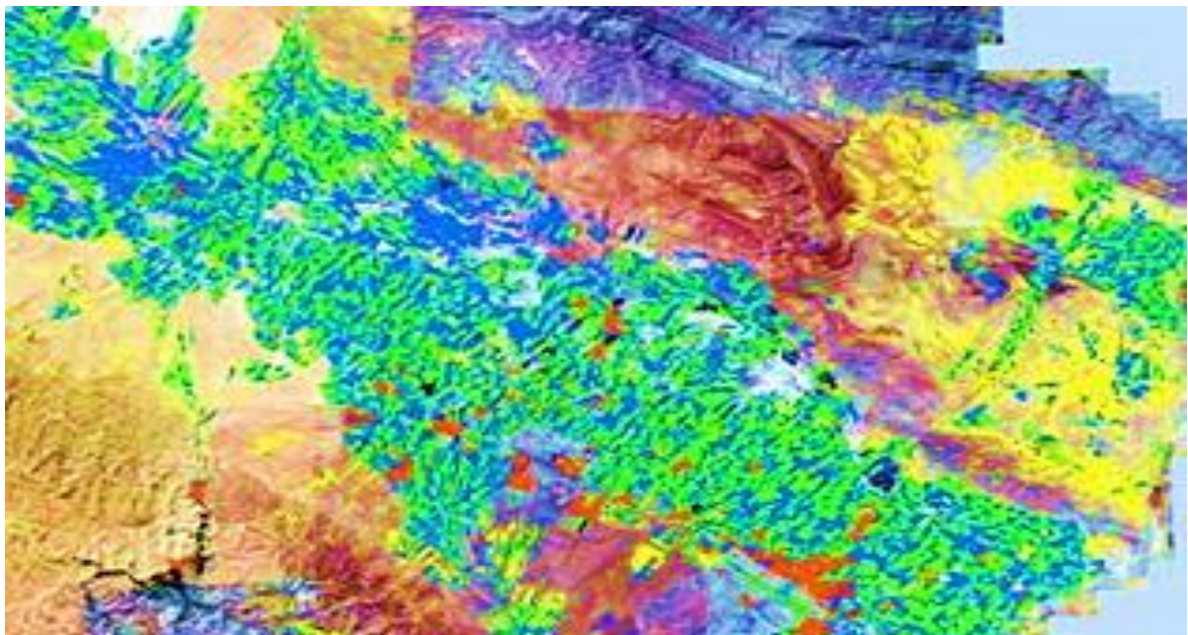


Fig. 10: The wheat cover map as reference for target detection where wheat fields are shown with green color.

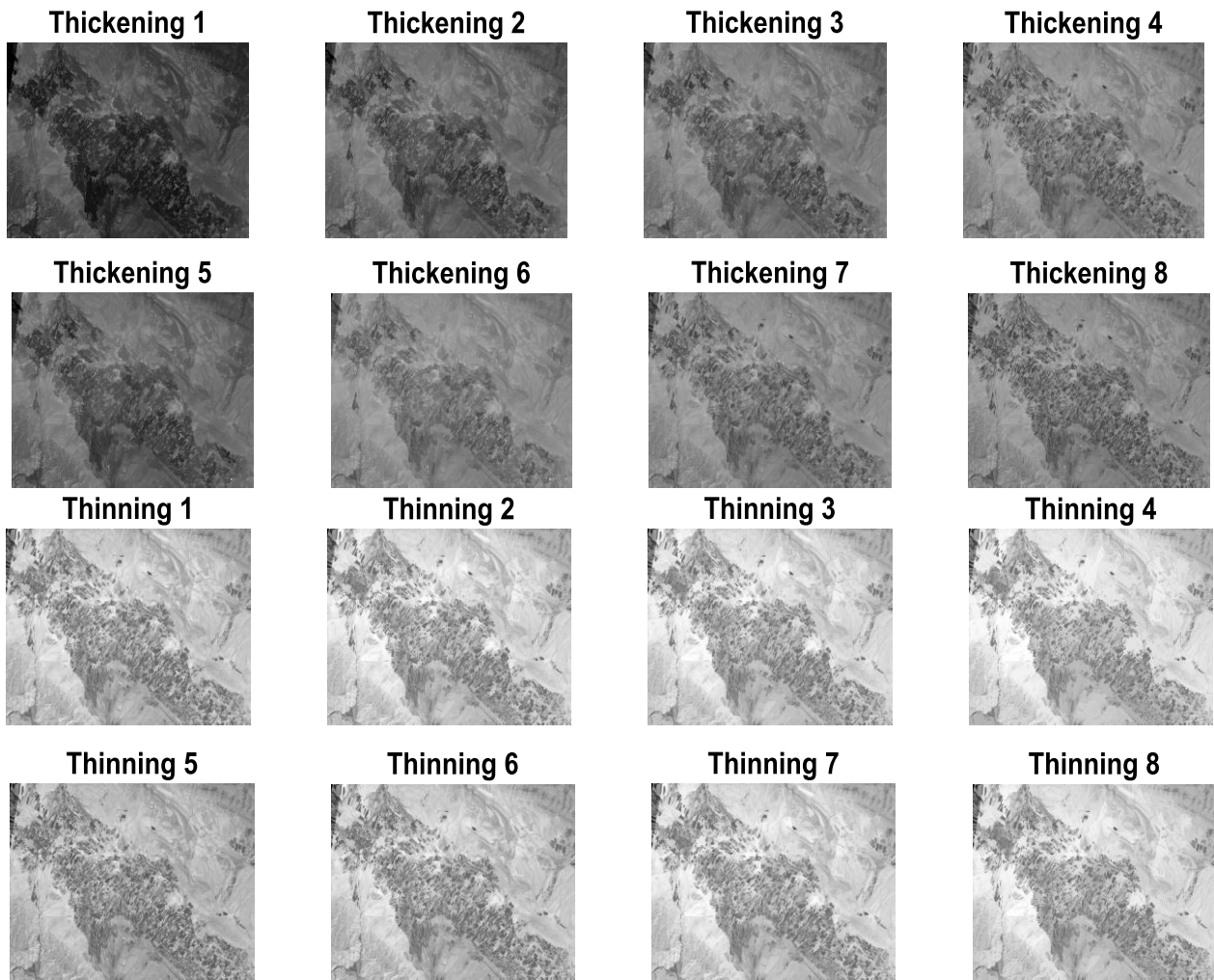


Fig. 11: Output images of thinning and thickening filters.

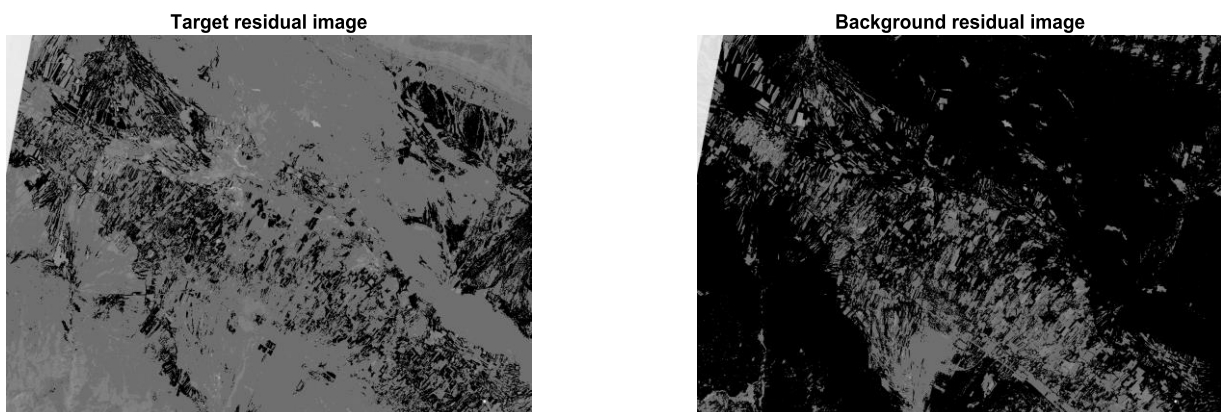


Fig. 12: The residual images.

Table 3: AUC values and running time of different detectors in the second group

Method	DTD-KSAM	AP-CR
AUC	79.88	96.09
Computation time (seconds)	68.44	6428.38

Table 4: AUC values and running time of different detectors obtained by spectral cube

Method	SAM	KSAM	CEM	DTD-KSAM	AP-CR
AUC	70.54	69.21	82.51	79.88	96.09
Computation time (seconds)	8.41	40.92	52.19	68.44	6428.38

Table 5: AUC values and running time of different detectors obtained by spectral-spatial cube

Method	SAM	KSAM	CEM	DTD-KSAM	AP-CR
AUC	75.62	72.57	85.06	78.47	93.20
Computation time (seconds)	8.85	38.07	94.51	65.38	6509.83

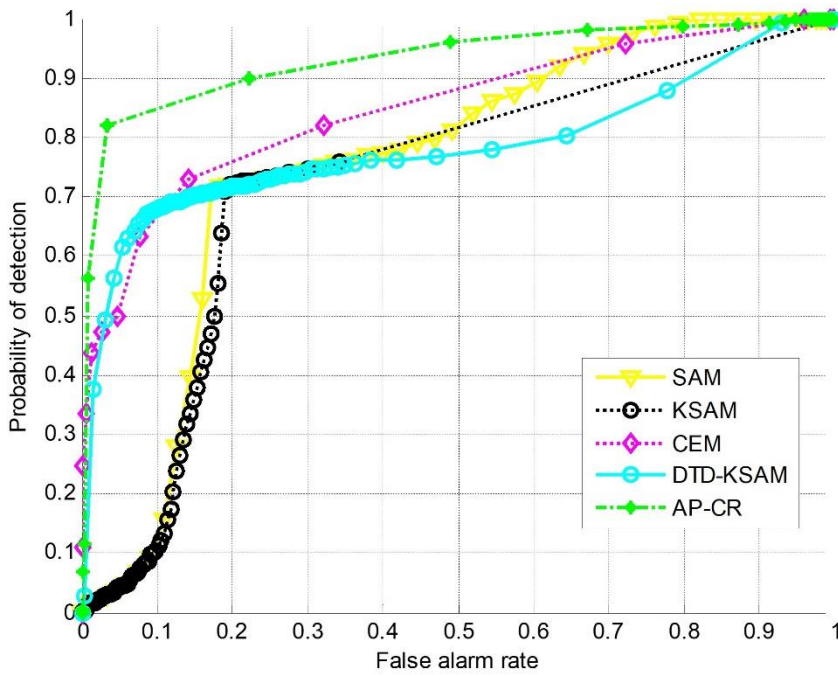


Fig. 13: ROC curves obtained by spectral-spatial cube.

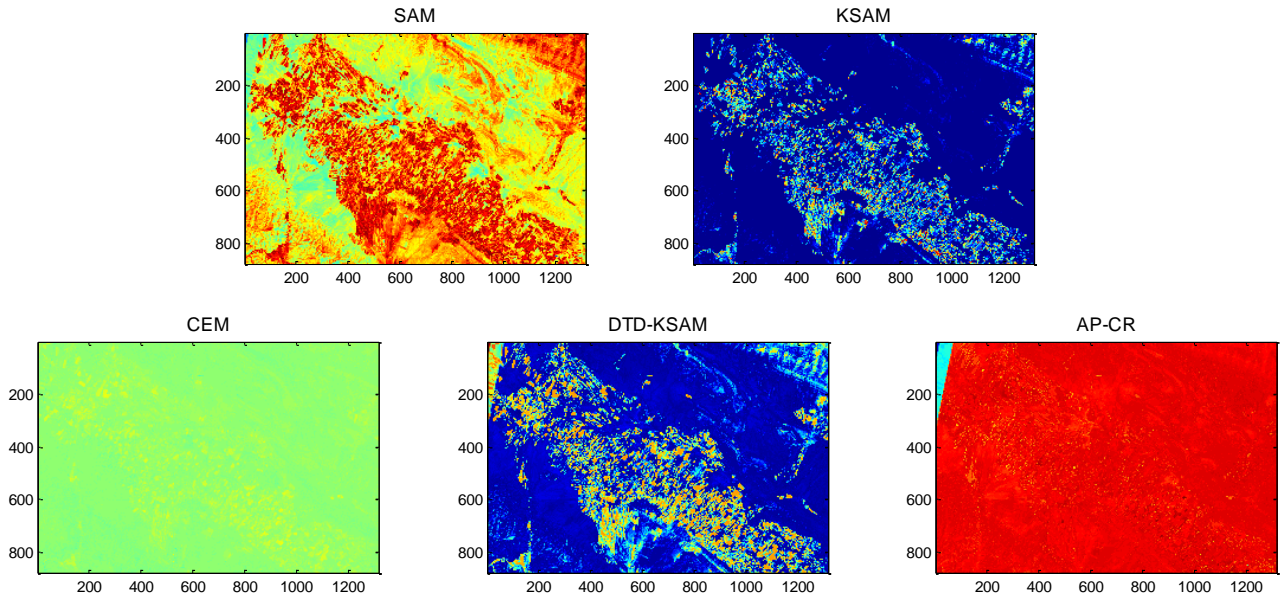


Fig. 14: Detection maps obtained by spectral-spatial cube.

As said before, the binary detection map is obtained through applying a threshold value. With considering each threshold value, a different binary map is achieved. Let $r1 = [D(y_1), D(y_2), \dots, D(y_N)]$ be the output detection for all N pixels of image. At first, the threshold value is selected by:

$$thr = \max(\max_{i=1:N} D(y_i)) \times const \quad (16)$$

where $const$ is a constant value. For instance, the binary detection maps of AP-CR obtained by $const = 0.001, 0.005, 0.01, 0.05, 0.1, 0.5$ are shown in Fig. 15. As

seen, by selection of a smaller threshold value, more details of image are labeled as target while by considering a larger value for threshold, lower points are assigned to the target class. By doing more experiments, another formula for selection of appropriate threshold is obtained:

$$thr = \min_{i=1:N} D(y_i) + 0.91(\max_{i=1:N} D(y_i) - \min_{i=1:N} D(y_i)) \quad (17)$$

The obtained binary detection map by using the above threshold is shown in Fig. 16 that is very close to the reference image of Fig. 10.

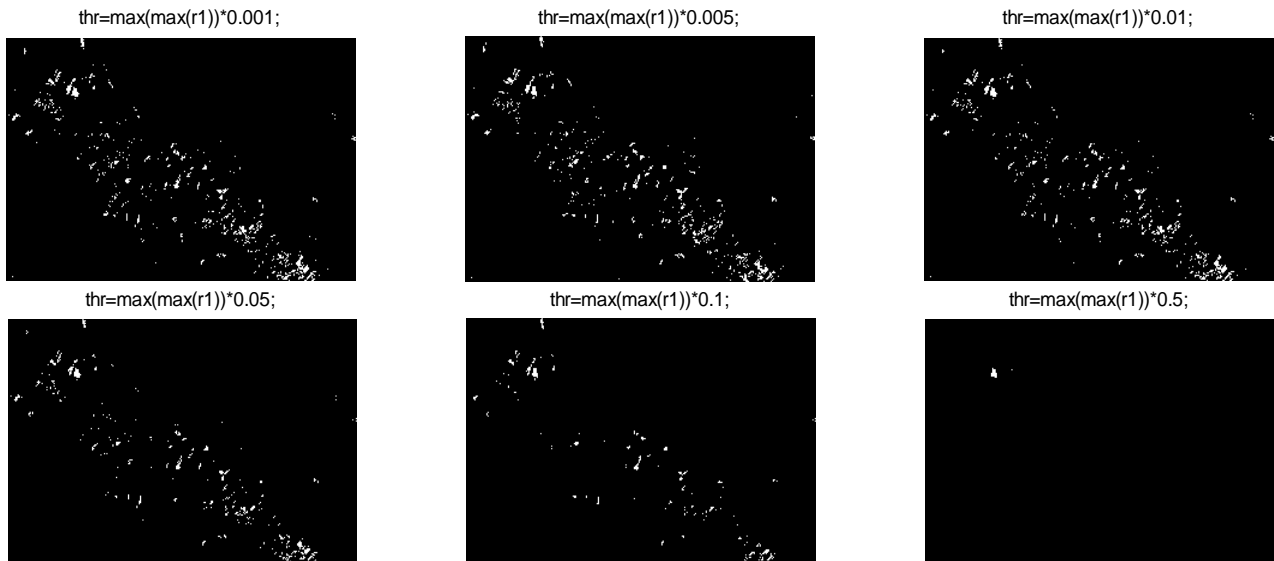


Fig. 15: Binary detection maps of AP-CR obtained by different thresholds.

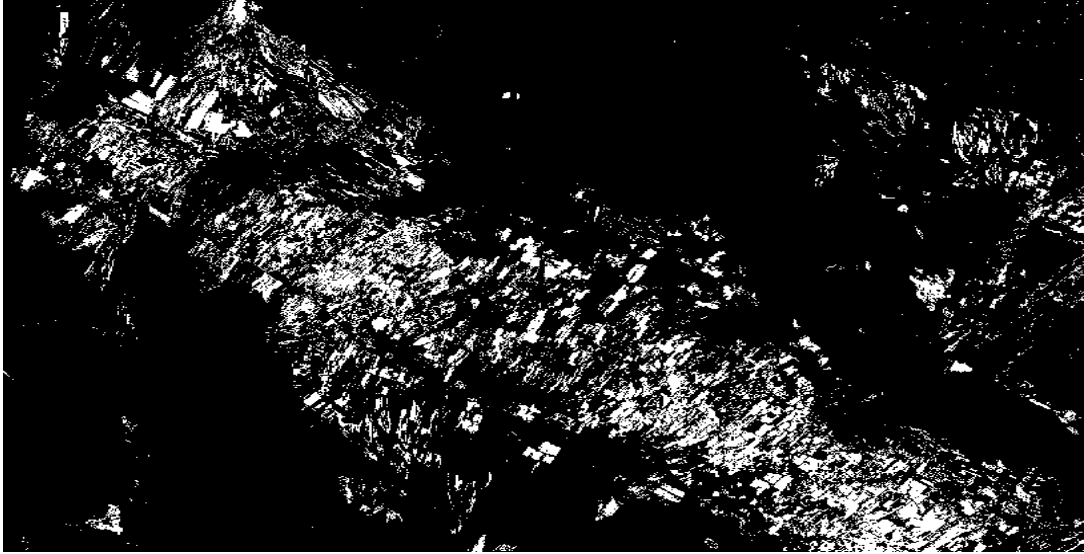
Binary Detection Map, $\text{thr}=\text{minr}+0.91*(\text{maxr}-\text{minr})$;

Fig. 16: Binary detection maps of AP-CR obtained by the chosen threshold.

Conclusion

Different hyperspectral target detectors such as SMF, MSD, ASD, OSP, SAM, KSAM, CEM, STD, DTD-KSAM and AP-CR are assessed for MS target detection in this work. Among different detectors, AP-CR is selected for MS target detection. The high performance of AP-CR is due to extraction of flexible attribute characteristics and the use of collaborative representation for approximation of each image pixel. In the collaborative representation, two individual subspaces for target and background classes are considered. The thinning profile containing details is used for composing the target subspace while the background subspace is generated by the thickening profile. The experimental results show the superior performance of AP-CR compared to other detectors whether they are applied to the original MS cube (containing just spectral features) or to the spectral-spatial cube that is result of stacking morphological profile on the MS image. Although the AP-CR method provides the highest accuracy, it needs a high running time compared to other detectors.

Author Contributions

Maryam Imani has all roles of ideation, data collecting, experiments designing, data analyzing, results interpreting, and writing the manuscript.

Acknowledgment

The author would like to thank the anonymous reviewers for their valuable comments for improving the paper.

Conflict of Interest

The authors declare no potential conflict of interest regarding the publication of this work. In addition, the

ethical issues including plagiarism, informed consent, misconduct, data fabrication and, or falsification, double publication and, or submission, and redundancy have been completely witnessed by the authors.

Abbreviations

<i>MS</i>	Multispectral
<i>SMF</i>	Spectral matched filter
<i>SAM</i>	Spectral angle mapper
<i>MSD</i>	Matched subspace detector
<i>OSP</i>	Orthogonal subspace projection
<i>CEM</i>	Constrained energy minimization
<i>ASD</i>	Adaptive subspace detector
<i>STD</i>	Sparsity based target detector
<i>KSAM</i>	Kernel based SAM
<i>DTD</i>	Difference based target detection
<i>AP-CR</i>	Attribute profile based collaborative representation
<i>ROC</i>	Receiver operating characteristic

References

- [1] S.W. Murphy, C.R.D.S. Filho, R. Wright, G. Sabatino, R.C. Pabon, "HOTMAP: Global hot target detection at moderate spatial resolution," *Rem. Sens. Environ.*, 177: 78-88, 2016.
- [2] M. Imani, "Sparse and collaborative representation-based anomaly detection," *SIViP*, 14: 1573-1581, 2020.
- [3] T. Guo, F. Luo, L. Zhang, B. Zhang, X. Tan, X. Zhou, "Learning Structurally Incoherent Background and Target Dictionaries for Hyperspectral Target Detection," *IEEE J. Sel. Top. Appl. Earth Obs. Remote Sens.*, 13: 3521-3533, 2020.
- [4] U. Kanjir, H. Greidanus, K. Oštir, "Vessel detection and classification from spaceborne optical images: A literature survey," *Remote Sens. Environ.*, 207: 1-26, 2018.
- [5] Y. Ma, J. Han, J. Liu, Y. Zhang, L. Bai, "A multi-scaled hierarchical structure model for multispectral image detection," *Signal Process. Image Commun.*, 47: 193-206, 2016.
- [6] B. Melville, A. Fisher, A. Lucieer, "Ultra-high spatial resolution fractional vegetation cover from unmanned aerial multispectral

- imagery," *Int. J. Appl. Earth Obs. Geoinf.*, 78: 14-24, 2019.
- [7] Z. Zhao, Y. Zhang, L. Bai, Y. Zhang, J. Han, "Multispectral target detection based on the space-spectrum structure constraint with the multi-scale hierarchical model," *Signal Process. Image Commun.* 68: 58-67, 2018.
- [8] F.C. Robey, D.R. Fuhrmann, E.J. Kelly, R. Nitzberg, "A CFAR adaptive matched filter detector," *IEEE Trans. Aerosp. Electron. Syst.*, 28(1): 208-216, 1992.
- [9] F.A. Kruse et al., "The spectral image processing system (SIPS) interactive visualization and analysis of imaging spectrometer data," *Rem. Sens. Environ.*, 44(2): 145-163, 1993.
- [10] L.L. Scharf, B. Friedlander, "Matched subspace detectors," *IEEE Trans. Signal Process.* 42(8): 2146-2157, 1994.
- [11] J.C. Harsanyi, C.I. Chang, "Hyperspectral image classification and dimensionality reduction: an orthogonal subspace projection approach," *IEEE Trans. Geosci. Remote Sens.*, 32(4): 779-785, 1994.
- [12] C.-I. Chang, D.C. Heinz, "Constrained subpixel target detection for remotely sensed imagery," *IEEE Trans. Geosci. Remote Sens.*, 38(3): 1144-1159, 2000.
- [13] S. Kraut, L.L. Scharf, L.T. McWhorter, "Adaptive subspace detectors," *IEEE Trans. Signal Process.*, 49(1): 1-16, 2001.
- [14] Y. Chen, N.M. Nasrabadi, T.D. Tran, "Sparse representation for target detection in hyperspectral imagery," *IEEE J. Sel. Topics Signal Process.*, 5(3): 629-640, 2011.
- [15] G. Camps-Valls, "Kernel spectral angle mapper," *Electron. Lett.*, 52(14): 1218-1220, 2016.
- [16] M. Imani, "Difference based target detection using mahalanobis distance and spectral angle," *Int. J. Remote Sens.*, 40(3): 811-831, 2019.
- [17] M. Imani, "Attribute profile based target detection using collaborative and sparse representation," *Neurocomputing*, 313: 364-376, 2018.
- [18] L. Zhang, L. Zhang, D. Tao, X. Huang, B. Du, "Hyperspectral remote sensing image subpixel target detection based on supervised metric learning," *IEEE Trans. Geosci. Remote Sens.*, 52(8): 4955-4965, 2014.
- [19] Y. Dong, L. Zhang, L. Zhang, B. Du, "Maximum margin metric learning based target detection for hyperspectral images," *ISPRS J. Photogramm. Remote Sens.*, 108: 138-150, 2015.
- [20] M. Imani, "RX anomaly detector with rectified background," *IEEE Geosci. Remote Sens. Lett.*, 14(8): 1313-1317, 2017.
- [21] T. Zhang, Z. Peng, H. Wu, Y. He, C. Li, C. Yang, "Infrared small target detection via self-regularized weighted sparse model," *Neurocomputing*, 420: 124-148, 2021.
- [22] K. Bhardwaj, S. Patra, "An unsupervised technique for optimal feature selection in attribute profiles for spectral-spatial classification of hyperspectral images," *ISPRS J. Photogramm. Remote Sens.*, 138: 139-150, 2018.
- [23] M. Dalla Mura, J.A. Benediktsson, B. Waske, L. Bruzzone, "Morphological attribute profiles for the analysis of very high resolution images," *IEEE Trans. Geosci. Remote Sens.*, 48(10): 3747-3762, 2010.
- [24] L. Wang, M. Li, H. Ji, D. Li, "When collaborative representation meets subspace projection: A novel supervised framework of graph construction augmented by anti-collaborative representation," *Neurocomputing*, 328: 157-170, 2019.
- [25] M. Imani, H. Ghassemian, "Weighted joint collaborative representation based on median-mean line and angular separation," *IEEE Trans. Geosci. Remote Sens.*, 55(10): 5612 - 5624, 2017.
- [26] M. Azadbakht, D. Ashourloo, H. Aghighi, H., S. Radiom, A. Alimohammadi, "Wheat leaf rust detection at canopy scale under different LAI levels using machine learning techniques," *Comput. Electron. Agric.*, 156: 119-128, 2019.
- [27] J.G.A. Barbedo, J. G.A., E.M. Guarienti, C.S. Tibola, "Detection of sprout damage in wheat kernels using NIR hyperspectral imaging," *Biosyst. Eng.*, 175: 124-132, 2018.
- [28] C.E. Dogan, N. Cebi, A. Develioglu, E.O. Olgun, E. O., O. Sagdic, "Detection of cysteine and cysteine in wheat flour using a robust LC-MS/MS method," *J. Cereal Sci.*, 84: 49-54, 2018.
- [29] Y. Seo, K.-s, Shin, "Hierarchical convolutional neural networks for fashion image classification," *Expert Syst. Appl.*, 116: 328-339, 2019.
- [30] Y. Zhong, X. Han, L. Zhang, "Multi-class geospatial object detection based on a position-sensitive balancing framework for high spatial resolution remote sensing imagery," *ISPRS J. Photogramm. Remote Sens.*, 138: 281-294, 2018.
- [31] E. Oguşlu, K. Islam, D. Perez, V.J. Hill, W.P. Bissett, R.C. Zimmerman, J. Li, "Detection of seagrass scars using sparse coding and morphological filter," *Remote Sens. Environ.*, 213: 92-103, 2018.
- [32] M. Imani, H. Ghassemian, "Attribute profile based feature space discriminant analysis for spectral-spatial classification of hyperspectral images," *Comput. Electr. Eng.*, 62: 555-569, 2017.

Biographies



Maryam Imani received the B.Sc. and M.Sc. degrees in electrical engineering from Shahed University, Tehran, Iran, and the Ph.D. degree in electrical engineering from Tarbiat Modares University, Tehran, Iran in 2009, 2011, and 2015 respectively. She continued her research in Tarbiat Modares University as a postdoc. She is an Assistant professor of the Faculty of Electrical and Computer Engineering at Tarbiat Modares University, Tehran, Iran. Her research interests include pattern recognition, signal and image processing, information analysis, and remote sensing.

Copyrights

©2021 The author(s). This is an open access article distributed under the terms of the Creative Commons Attribution (CC BY 4.0), which permits unrestricted use, distribution, and reproduction in any medium, as long as the original authors and source are cited. No permission is required from the authors or the publishers.



How to cite this paper:

M. Imani "Target detection using multispectral images, a case study: wheat detection in chenaran county in iran," *J. Electr. Comput. Eng. Innovations*, 9(1): 11-24, 2021.

DOI: [10.22061/JECEI.2020.7455.394](https://doi.org/10.22061/JECEI.2020.7455.394)

URL: http://jecei.sru.ac.ir/article_1479.html

